IEEE Open Journal of
Power Electronics

Received 13 June 2022; revised 22 July 2022; accepted 31 July 2022. Date of publication 3 August 2022;
date of current version 12 August 2022. The review of this article was arranged by Associate Editor Xiong Du.

*Digital Object Identifier 10.1109/OJPEL.2022.3196134*

# End-of-Life Detection of Power Electronic Converters by Exploiting an Application-Level Health Precursor

**MARTIN VANG KJÆR (Student Member, IEEE), HUAI WANG (Senior Member, IEEE), AND FREDE BLAABJERG (Fellow, IEEE)**

Energy, Aalborg Universitet, 9220 Aalborg, Denmark

CORRESPONDING AUTHOR: MARTIN VANG KJæR (e-mail: mkj@energy.aau.dk)

This work was supported by the Villum Fonden.

**ABSTRACT** Extensive studies have been conducted in regards to estimating the useful life of power electronic converters in order to prevent failure related downtime. The state-of-the-art of converter reliability is based on the physics-of-failure approach, which involves some concerns such as the uncertainty introduced by extrapolating the accelerated test results to other usage conditions, which results in failure probability distributions inhibiting a variance of several years. In order to overcome this issue, the state-of-the-art is currently seeing an increase in research output, which are in favour of basing the reliability studies on physics-of-degradation based methods. The existing methods are restricted to only consider a single component and due to the impracticability of monitoring each single component, there is an essential need for methods, which can monitor the health state of the entire converter. This paper proposes a method which uses the converter operating efficiency to monitor parameter shifts of multiple components, which can be used to gain precision when stating the converter lifetime. A supervised classifier is used to detect the end-of-life while simultaneously coping with the fundamental issue of the loading influencing the efficiency. The method proves to have high accuracy even when measuring inaccuracies are taken into account.

**INDEX TERMS** Condition monitoring, end-of-life detection, health precursor, maximal margin classifier, power electronics, supervised learning, support vector machine.

## I. INTRODUCTION

Power electronic converters are being extensively used in a wide area of applications and is indisputably a key enabling technology in the current transition towards transforming the global energy sector from fossil-based to zero-carbon [1]. Due to the high cost of failure related downtime of renewable generators, considerable efforts have been made to assess the reliability of power electronic converters [2]. The state-of-the-art of the assessment methods is based on the physics-of-failure (PoF) approach, which utilizes the knowledge of the converters life-cycle loading and the potential failure mechanisms in order to assess the time-to-failure [3]. While the PoF methodology seems as a good approach for systems with sufficient legacy there are still some concerns, which can lead to inaccurate lifetime predictions. One common concern is the tendency of inherently base the prediction on one single failure mechanism, which is an idealistic assumption since in reality several failure mechanism could be co-existing and some could even be related in terms of sharing the driving forces that govern multiple failure mechanisms [4]. Furthermore, the extensive use of Miner's rule for linear damage accumulation is a simplistic assumption, as this does not consider the interactions that leads to positive feedback of the driving forces of failure causing the evolution of damage to accelerate as the components degrade [5]. Still, the major concern linked to PoF is the establishment of the useful life of the components by means of extrapolating the accelerated test results to other usage conditions in order to obtain the failure fatigue model parameters. Extrapolating the test conditions to other usage conditions introduces uncertainty as the accelerated test data are often based on a restricted number of constant loading conditions, which differs significantly from

the real applied use [6], [7]. The loading profiles linked to renewable generation is of highly dynamical nature inhibiting a large variety of gradients and stress ranges, which significantly influences the mechanical stress that excites the failure mechanisms of power devices [8]. A common practice, to account for the issue of differing conditions, is to model the failure fatigue model parameters as distribution functions and thereby represent the lifetime prediction as a failure probability as described in [7]. When all possible uncertainties are considered, the resulting lifetime distribution tends to inhibit a variance compromising several years and does therefore end up lacking sufficient precision for any unique cases under study [9]. A common useful reliability metric when dealing with failure distributions, is the percentile life, which denotes, at which point in time a certain percentage of the distribution is accumulated. The correct percentage value to denote the end-of-life is application dependent, e.g., when considering power converters with the functionality of acting as interface between renewable energy sources and the power grid, a suitable percentile value would be of one or even less. Allowing the risk of a higher percentage of the generation units to enter a failed state is likely to lead to improper system operation. The stringent reliability requirements rightfully forces the consideration of only a small fraction of the distribution, when in reality any unique case could be located anywhere in the distribution.

An effective way to overcome the before mentioned issues is to exploit prognostics and health management (PHM) based methods, where the long term changes in the electro-thermal parameters are used as component health state indicators. The degradation of power electronic components will typically occur at the material or interconnection-level and as the changes of materials and interconnections influence the electro-thermal parameters they can indirectly signify the gradual wear-out of the components and thereby be harnessed to assess the current device condition [10]. The classical indicators compromise the increase in the forward voltage of an IGBT or diode and the thermal resistance of power devices. The variation of the forward voltage is influenced by temperature, gate oxide integrity, metalilization reconstruction and the quality of the electrical connections, namely bondwire fatigue and lift-off. The steady increase is an indication of the aluminium surface metalization influencing the ohmic resistance while sudden steep increases in the voltage drop can be observed when a bond wire lifts off. This is due to the fact that the remaining bondwires are now forced to carry an additional load [11]–[16]. On the other hand, the evaluation of the thermal resistance can be used to indicate the degradation in the form of solder or ceramic cracks that reduces the power modules ability to conduct heat from the power device and into the heat sink [11], [17], [18].

Based on the existing research, it is quite clear that exploiting these health indicators appears to be quite effective in terms of covering several types of degradation modes. Nevertheless, all existing methods are limited to one single type of component or an individual component [10], [19]–[21]. This is a severe limitation, as at the application-level the degradation is likely to occur in multiple components concurrently as a consequence of different types of occurring parameter shifts, which all adds up to the overall converter degradation. However, these mutual effects cannot be verified through the assumption that one single component degrades at a time and it would most certainly be a tedious affair, if not impossible, to estimate the health of every single component operating in the power converter. Also, due to the long and exhaustive process of locating and remedying any particular defect, it is highly unlikely that one component is replaced in case of component failure and it is therefore essential to monitor the health status of the entire converter using converter-level signals as alternative solutions [5]. This paper proposes a method, which utilizes the converter operating efficiency as a unified health precursor of the entire converter, and enables the assessment of the health status of the entire converter. The method can be used to gain precision, when stating the lifetime of power converters in terms of unique cases.

Still, for this method to be useful in terms of detecting when the converter has reached its end-of-life state, it is required that a critical level of degradation is defined. The main issue to overcome, when exploiting the efficiency as a health precursor, is that the efficiency is dependent on how the converter is loaded. Due to this loading dependency, a single discrete threshold will not do, as this will result in several overlapping efficiency outcomes for different levels of converter degradation. Finally, this paper additionally presents a method, which utilizes a binary supervised classifier that defines a safe operational area, and effectively constructs a boundary, which adapts to the specific loading condition. The efficiency based end-of-life detection methodology can be used to base the maintenance scheduling of power converters when operating in a large variety of applications. The outcome could be useful in terms of providing advanced warnings of failure with the purpose of minimizing unscheduled maintenance, extend the maintenance cycles and thereby reduce life-cycle cost by reducing failure related downtime.

## II. FRAMEWORK AND METHODOLOGY

In this section, a method which is used to detect the end-of-life of power converters is presented. The method exploits the degradation of multiple components concurrently while taking into account each possible operating condition and their respective impact on the unified health precursor, which signifies the practicability of the method. In order to illustrate the effectiveness of the proposed method, every consecutive step needed to obtain an end-of-life decision boundary, is presented via a case study using a common topology used for renewable power generation. The study is based on a solar based generation unit, in which the power processing is realized via a dual-stage PV-inverter as presented in Fig. 1. The PV-inverter consists of two stages, in where each stage is an assembly of numerous power electronic components. The three types of power electronic components, in which parameter shift is considered are the capacitors, the active

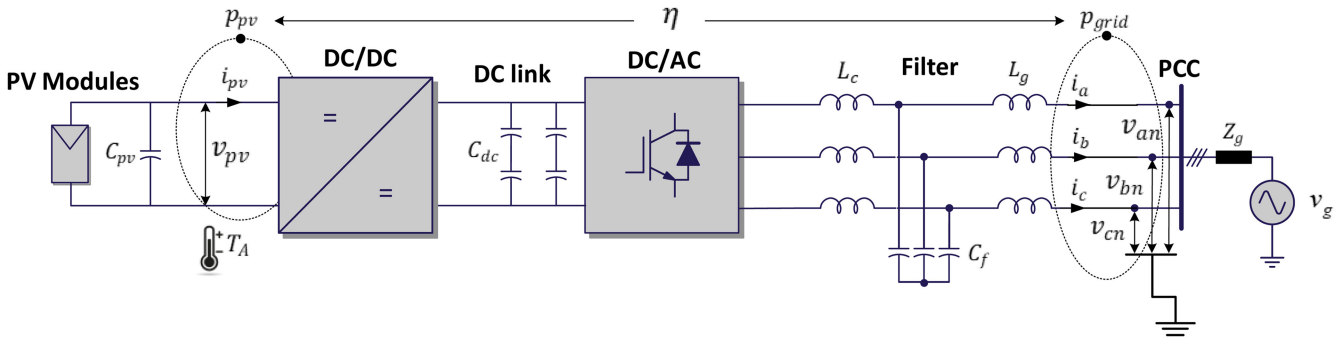


**FIGURE 1.** Solar based generation unit rated at 10 kVA used for the case study outlining the components considered for wear related degradation. $\eta$ denotes the efficiency when considering the power losses that occur from the input power $p_{pv}$ to the output power $p_{grid}$.

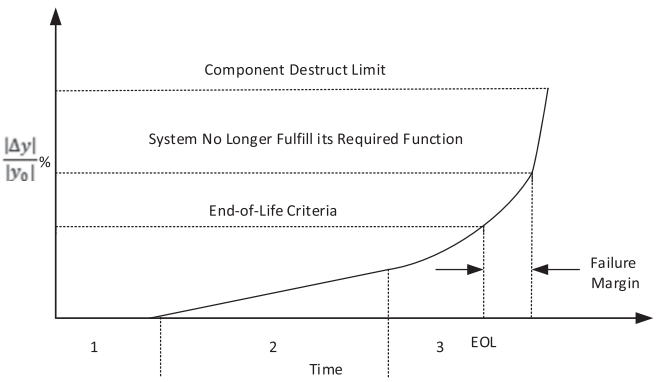


**FIGURE 2.** A generic degradation curve outlining the three typical stages of power electronic component degradation process. $\Delta y$ is the parameter drift of the given health precursor $y$, $y_0$ is the initial state of a component operating in a "as good as new" state.

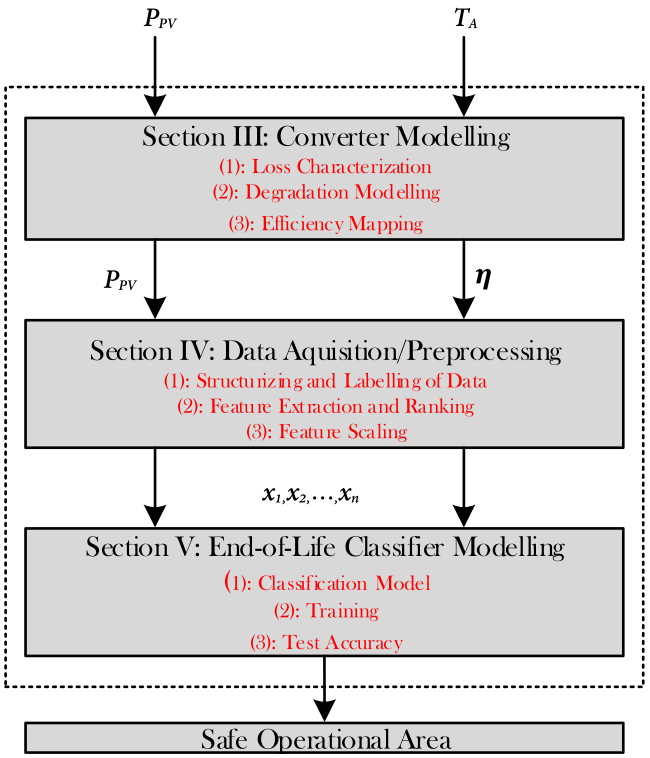


**FIGURE 3.** Framework linked to the proposed method and its paper sections.

power switches and the power diodes. The useful life of the respective components is dictated by an end-of-life criterion, which is defined based on some historical knowledge of the destruct limit and the inclusion of some margin in order to prevent failure related downtime. Fig. 2 presents a generic degradation curve of a health precursor, where $y$ is the monitored value of the given health precursor, $\Delta y$ is the parameter drift with respect to its initial value $y_0$. The y-axis shows the absolute value of the parameter change in percentage. A power electronic component usually has three distinctive stages that are prominent during an entire degradation process. The stages compromises the ones labeled stage 1,2 and 3, that for each includes a time interval, where the health precursor either keeps constant, changes linearly, increases or decreases at an accelerated pace respectively. The allowed efficiency change considered in this study, is based on the large share of existing studies on condition monitoring of individual components. Meaning, that the end-of-life state is reached when the efficiency change of the converter caused by the combined component parameter shifts. A 20% increase in the forward voltage is chosen as this is consistent with the general consensus of the allowed degradation in existing studies [22], whereas a 2-3 times increase of the ESR of electrolytic capacitors are commonly used [5]. The number of components, which constitute each conversion stage and the maximum allowed individual parameter change are listed in Table 1.

The framework linked to the proposed method is outlined in Fig. 3, which compromises three main parts, i.e., the initial part involves the converter modelling in terms characterizing the losses and how they are effected by component degradation. The input power and the output are obtained for any possible operating condition and the efficiency is then computed and mapped. The long term efficiency can then be obtained by use of the mapped values and real field mission

**TABLE 1. Power Electronic Components and their Respective Assigned Parameter Shifts**

| Component type | DC/DC stage | DC link | DC/AC Stage |
|---|---|---|---|
| Active Power Switches (20% increase in $V_{CE,on}$) | 1 | - | 6 |
| Power Diodes (20% increase in $V_F$) | 1 | - | 6 |
| Capacitors (300% increase in ESR) | - | 4 | - |

profiles, which enables the emulation of a range of realistic usage conditions. The second part compromises the acquisition and handling of the data, in terms of forming a data ensemble for managing the data so that it is compatible with the applied classification algorithm. The most discriminating signal characteristics of the data ensemble is then identified for use for yielding maximum classifier performance. Subsets of the signal characteristics are used to train and test the performance of the end-of-life classifier and finally, the effectiveness of the method is proven by visualizing a distinct separation of the converters, which has reached its end-of-life state from those which have not via a defined safe operational area.

## III. CONVERTER CHARACTERIZATION

In this section, the factors which indirectly enables the use of efficiency as a health precursor are briefly characterized. The main idea is to exploit the fact that the power conversion will become less efficient as the components degrade and an end-of-life criteria can therefore be stated based on the degraded efficiency. The common wear-out indicators of the active and passive power devices, i.e., the on-state voltage and the forward voltage will both directly influence the dissipated losses. The considered power loss $P_{Loss}$ can be classified into the following six categories; the switching loss $P_{SW}$ and the conduction loss $P_{Cond}$ which are both produced by the passive and active power devices, the ESR losses $P_{ESR}$ of the DC-link and the AC capacitors, the gate charge losses $P_{Gate}$, and the magnetic copper losses $P_{Copp}$ of the filter inductors. It is assummed that only the passive and active power devices and the DC-link capacitors, i.e. the conversion stage components are exposed to parameter drift and thereby contribute to the change in efficiency. The remaining losses, with the exception of the iron losses of the magnetics, are considered but are assummed to be to be the same throughout the life-cycle of the converter. Fig. 4 presents the classification of the considered power loss components, where the red color denotes the components considered for parameter drift. The relationship among the power loss components, shown in Fig. 4 leads to the following equation

$$\begin{aligned} P_{Loss} &= P_{Gate} + P_{SW} + P_{ohm} \\ &= P_{Gate} + P_{SW} + P_{Cf} + P_{Copp} + P_{Cond} \end{aligned} \tag{1}$$

The ohmic loss $P_{ohm}$ is produced in the power circuit and is proportional to the square of the rms value of the current. It can be divided into the respective losses of the ESR and the damping resistance $P_{Cf}$, the copper loss $P_{Copp}$ and the conduction loss $P_{Cond}$.

The output characteristics of the power devices and thereby the efficiency is dependent on multiple factors, including

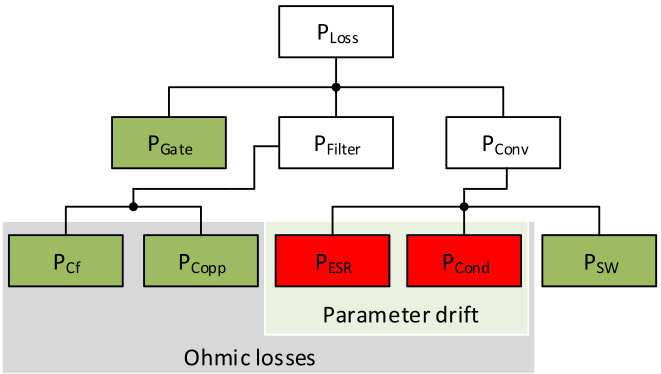


**FIGURE 4. Classification of the 6 power loss components, where the red colored boxes, denotes the components which are considered to have a change in the amount of dissipated losses as these components degrade. $P_{Conv}$ is the total loss at the conversion stage. $P_{Filter}$ is the total loss dissipated in the AC filters and $P_{Cf}$ denotes the combined losses caused by the ESR and the damping resistance of the filter capacitors.**

loading and temperature, a single value threshold can not be based on the lowered efficiency. The output characteristics for healthy units is mapped according to the manufacturing data and additionally the component-level condition indicators are manipulated in terms of small increments until the degradation limits presented in Table 1 is reached. In regards to the factors that influence the efficiency and that are not ageing related, the output characteristics of the active power switches and the power diodes are shown in Fig. 5. As shown in Fig. 5(a) and (b), there are regions that exhibit near linear-relationship, but also some which are highly non-linear. These different regions, will have a different impact on the operating efficiency. For example, the region that displays a nearly linear proportional relationship will prove to be highly insensitive to load changes, but due to the large variety of operating conditions linked to renewable generation, it is highly unlikely that the converter is operated solely in that region. Due to the multivariate dependency, the output characteristics is mapped using a 3D lookup table as exemplified for active power devices in Fig. 6, where $I_C$ denotes the localized loading and $T_J$ denotes the junction temperature of the device. The mission profile dependent applied converter loading can be obtained as outlined in [23], whereas the localized loading and the junction temperature can be obtained as described in [24].

In case of the wear related degrading of the DC-link capacitors and their impact on lowering the converter performance, the long term change in the equivalent series resistance (ESR) will impact the dissipated losses, which can be computed as

$$P_{Loss,cap} = ESR(T, f) \cdot I_{RMS}^2(f) \tag{2}$$

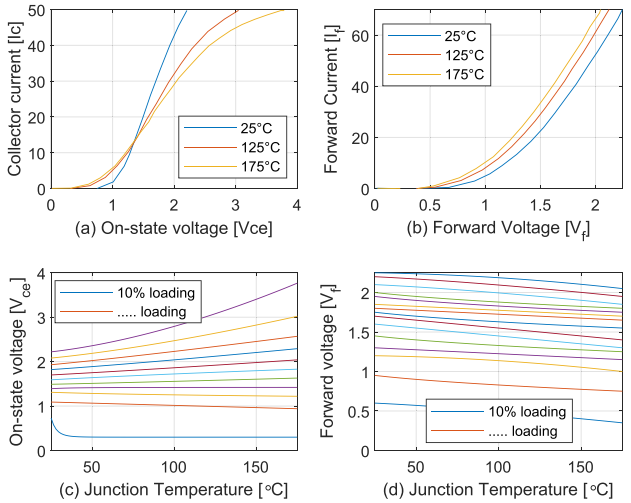


**FIGURE 5.** The output characteristics of the active switches and the power diodes outlining the efficiency dependence on loading and temperature. (a): output characteristics of the active switches. (b): output characteristics of the power diodes. (c): The on-state voltage dependence on temperature. (d): The forward voltage dependence on temperature.

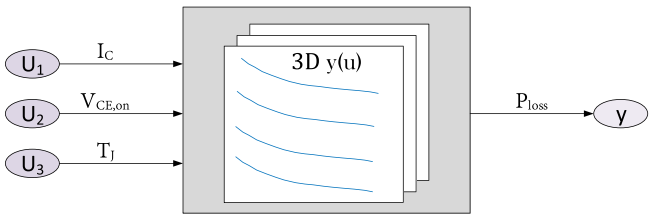


**FIGURE 6.** 3D lookup table used to map the output characteristics of the active power devices of the DC/DC and DC/AC stage.

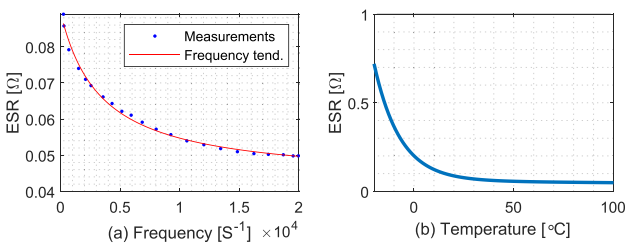


**FIGURE 7.** (a) and (b): Adapted frequency and temperature dependency of the equivalent series resistance of the studied DC-link capacitors.

where $I^2_{RMS}(f)$ denotes the RMS value of the ripple current components and $T$ denotes the capacitor hotspot temperature. As it is evident from expression (2), the ESR does contain some temperature and frequency dependency and as shown in Fig. 7(a), the ESR value has a decreasing tendency with increasing frequency. The lowering in the ESR value is even more pronounced with the increase of temperature as shown in Fig. 7(b), that shows the ESR tendency, which is more or less general for electrolytic capacitors. Both dependencies needs to be considered, as they will impact the amount off losses dissipated in the DC-link capacitors. Analogues to the case of the power devices, the losses are characterized for each

**TABLE 2.** The Electrical Parameters of the AC Filter and the Gate Driver, Which Influence the Power Loss of the Converter

| | | |
|---|---|---|
| Power rating | $P_{rated}$ | 6 kW |
| Switching frequency | $f_{sw}$ | 10 kHz |
| Filter resistance | $R_f$ | 0.2 Ω |
| Filter resistance (grid side) | $R_{fg}$ | 0.1 Ω |
| Damping resistance | $R_d$ | 1 Ω |
| Total gate charge | $Q_g$ | 0.395 μC |

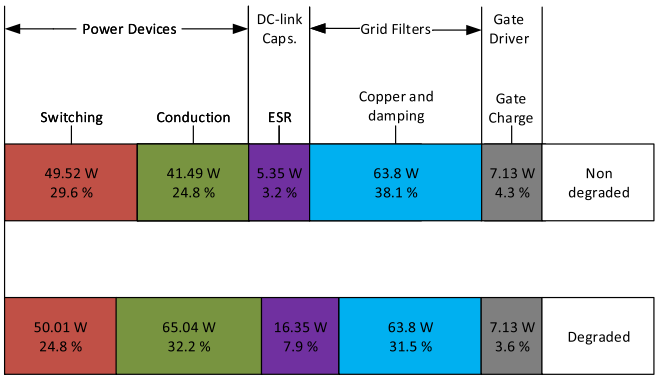


**FIGURE 8.** Power loss breakdown for non degraded and degraded states of the components considered for parameter drift. The power loss breakdown is conducted at 6 kW, 10 kHz operation.

loading, temperature and frequency condition as documented in [25]. In order to gain some insight in how the component losses is affected by the degradation and in which proportion, each of the parameters contribute to the change in efficiency, a power loss breakdown is conducted. The electrical parameters of the AC filter and the gate driver that is used for the circuit simulations is presented in Table 2 and the results of the power loss breakdown is shown in Fig. 8. As shown in Fig. 8, the conduction losses of the power devices accounts for the majority of the efficiency change and constitute nearly one-third of the total power losses in the degraded state, which is more than a 7% increase of their respective proportion in respect to the non-degraded state. The loss contribution caused by the degradation of the DC-link capacitors, do also show a significant change by more than doubling its contribution to the overall power losses. Finally, the wear related degradation is modelled by an incremental increase of ESR until it reaches the defined parameter shift criterion listed in Table 1. Based on the loss characterization and the degradation modelling, the long term efficiency profile can be computed based on real field mission profiles in order to emulate the data related to real operational usage. Additionally, regardless of which conditions that imposes the unit, the efficiency can be obtained for the entire defined health spectre as depicted in Fig. 9, where one specific operating condition results in different efficiency response due to varying health states. The gained opportunity of acquiring efficiency responses for every possible operation and health state enables the possibility of creating large multifaceted datasets required for the condition monitoring algorithm design.

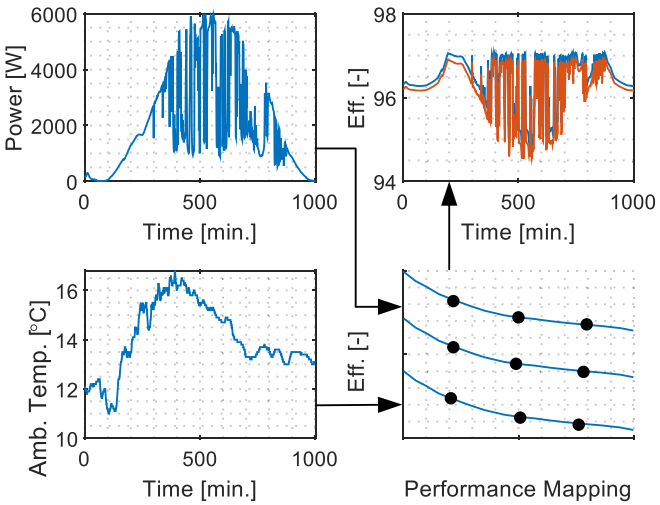


**FIGURE 9.** Enabling of long-term efficiency responses by use of performance mapping of each operating and health condition.

**TABLE 3.** Structure of the Dataensemble Created for End-of-Life Detection

| Member ID | Efficiency | Loading | Fault Code |
|---|---|---|---|
| 1 | $6000x1$ Time series data | $6000x1$ Time series data | 1 |
| 2 | $6000x1$ Time series data | $6000x1$ Time series data | 0 |
| ... | ... | ... | ... |
| 70 | $6000x1$ Time series data | $6000x1$ Time series data | 0 |

## IV. DATA ACQUISITION AND PRE-PROCESSING

Regardless of the used health precursor, data analysis is the foundation of any condition monitoring activity. In this section, a dataensemble is created for managing and labelling of the large dataset, which is required for the development of the end-of-life detection algorithm. The requirements for the dataensemble is that it represents a lifetime record of system operation i.e., run-to-failure data. In addition of covering the entirety of health states, it is also required to cover all variations of operating conditions, as this also has a direct influence on the health precursor. Finally, it is required that the data is organised so that the condition monitoring algorithm can keep track of the large of amount of data in terms of which conditions the data represents.

Based on the listed considerations and requirements the family of data sets consists of 70 members, including members of which the unit is operating in a "as good as new" state or partially degraded. This share of members are assigned a binary condition code of zero. The remaining share of members represents the system operating in a fully degraded state and is assigned the binary condition code of one. Each member contains the data variables i.e., signal data of the efficiency and loading of the generation unit and each data variable consists of time series data with 6000 samples covering approximately four days. The structure of the dataensemble is depicted in Table 3. While the raw data managed, it is still required to process the raw signal data into numerical features, which

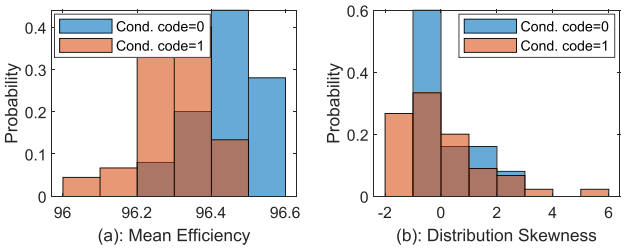


**FIGURE 10.** Histograms for visualization of condition based feature separation.

will yield optimal condition monitoring algorithm classification results, while still preserving the information contained in the original data ensemble. As the signal features are extracted manually, it is required to apply a method, which effectively can identify the features of the data, that is of high relevance. More specifically, identify signal features whose behaviour changes in a predictable manner as the converter degrades and at the same time discarding the irrelevant ones as these can contribute to overfitting of the model and thus leading to biased classification outcomes. The filter based feature selection method for binary classification evaluates the individual features in terms of the degree of separation of the defined classes. In other words, the optimal features are regarded as the ones which are useful to distinguish new and partial degraded conditions from the end-of-life conditions by exhibiting as little overlapping as possible by clustering the similar conditions together. Initially, a preliminary assessment of how the effectiveness of each feature is carried out by means of feature histograms visualization. Histograms allows one to get an early sense of feature effectiveness and thereby get a good impression of which subset of features are worth to include in the more rigorous quantitative assessment using the filter methods. The histogram plot visualizes the separation between the labeled groups of the defined data ensemble by binning the feature data and by using colors to identify, which binary condition code the data belongs to. This is exemplified in Fig. 10, where the separation of the feature variables mean efficiency and distribution skewness of the units operating efficiency is shown. In both plots, the value of 0 (blue) indicates a fully healthy or partially degraded system operation and a value of 1 (orange) indicates a system operating at the end-of-life state. As seen in the histogram representing the mean efficiency, it shows that most of the healthy feature data are located within the range of the two far-right bins, whereas most of the fully degraded data lies within the remaining bins. Despite that is does not exhibit total separation, the mean efficiency might work well in a combination with a feature containing information of the applied loading conditions. By contrast, the histogram representing the distribution skewness exhibits highly overlapping feature data and the particular bins, which do not show any overlapping are at the extremes of both high and low values, making the result ambiguous and therefore not useful for end-of-life-detection. It should be emphasized that regardless of the efficiency features chosen,

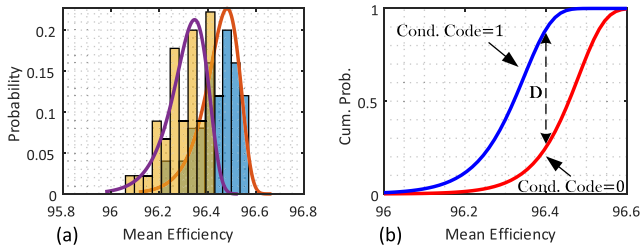


**FIGURE 11.** (a): Weibull distribution function fit of each classes of mean efficiency. (b): Corresponding cumulative distribution functions of the classes exhibiting good separation properties, by having a relatively large KS statistic.

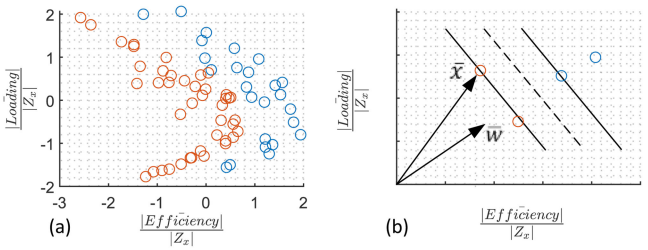


**FIGURE 12.** (a): Feature space where the red circles denotes fully degraded converter data and the blue circles denotes new or partially degraded converter data. (b): Concept of SVM where the margin is defined as the perpendicular distance between the decision boundary and the nearest data points. $\bar{w}$ is the weighting vector and $\bar{x}$ is a random data observation.

it is crucial that it is combined with an applied loading feature. In the case of e.g, peak efficiency it cannot be guaranteed that the peak condition of the loading/efficiency curve is reached during the low loading periods observed at winter time and excluding the load feature, would lead to false alarm and therefore no-failure related maintenance.

The final feature selection of the feature subset, that was chosen based on the histogram visualization, will be based on Kolmogorov-Smirnov (KS) test, which is simply a quantitative measure of the separation of the condition variable. The method is advantages in respect to the mean based methods due to the fact that two feature distributions can easily exhibit a large degree of overlapping even though their respective means differ due to the difference in distribution spread. The KS statistic is in essence the supreme of the difference between the distributions sampled from the two condition classes and it can be calculated as [26]

$$D = \sup_{x \in \mathbb{R}} |F_{cond.1}(x) - F_{cond.0}(x)| \tag{3}$$

where $D$ is the KS statistic; $F_{cond.0}$ and $F_{cond.1}$ are the cummulative distribution functions from the partially healthy and fully degraded classes respectively. The larger the KS statistic is, the lesser the likelyhood is that the data is sampled from the same distribution i.e, the two classes exhibit good separation. In Fig. 11, the fitted probability functions of each classes of the mean efficiency is shown alongside the computed supreme distance of the classes. Based on superior separation properties, the mean efficiency is chosen in combination with mean loading as the signal characteristics used for condition monitoring. However, before the feature data can be used for training of the classification algorithm, it is required to remove the relatively large difference in the dimensional level of variation of the loading and the efficiency. If the dimensions of the two features are not normalized to a similar level, it can result in biased classifier output to some of the large-scale loading data. This is due to the use of distance between data points in the development of the decision boundary and the fact that if one of the features has a broad range of values, the distance will be governed by this particular feature. The optimal choice of either scaling or standardization based methods depends on the application. In the case of clustering or distance based analyses, the z-score standardization can be the crucial choice for obtaining advantages results. The outcome of the z-score standardization is that the feature data will be rescaled so it will obtain the properties of a standard normal distribution. The standardized scores of the feature samples are calculated as follows

$$z_i = \frac{(x_i - \mu)}{\sigma} \tag{4}$$

where $\mu$ is the sample mean and $\sigma$ is the standard deviation from the mean.

## V. END-OF-LIFE CLASSIFIER MODELLING

With the most relevant features properly processed, it is now time to split up the feature space by use of a decision boundary. The decision boundary will be based on the support vector machine (SVM) algorithm, which makes use of the kernel trick to model the non-linear decision boundaries required in this case. When observing the feature space shown in Fig. 12(a), it is quite obvious that the health precursor data is not linearly separable i.e., no straight line can be drawn through the feature space, which divides all non fully degraded data from fully degraded ones. There may exist infinitely many solutions that can separate the health classes and so we should strive to obtain the one which gives the smallest generalization error. The SVM approaches this problem by means of the concept of margin, which is defined as the smallest distance between the decision boundary and any of the data samples, as illustrated in Fig. 12(b). In SVM the decision boundary is chosen as the one for which the margin is maximized [27]. The decision rule for the SVM makes use of the decision boundary and can be understood by considering the arbitrary observation point labelled $\bar{x}$ in Fig. 12(b). Now, for the sake of getting an indication of if the arbitrary observation point is located on the left or right side of the decision boundary, its corresponding vector is projected onto the weighting vector $\bar{w}$, which is perpendicular to the decision boundary. By performing this projection the distance in terms of a number that is proportional to $\bar{w}$, is obtained in the direction of $\bar{w}$. Considering this, a decision rule can be stated as

$$y(x) = w^T \phi(x) + b \tag{5}$$

where $\phi(x)$ denotes a feature-space transformation and b is the explicit bias parameter. For now, there is not enough constraints to fix the values of b and $\bar{w}$, which requires the definition of target values as $t_n \in -1, 1$, and that data points will be classified depending on the sign of $y(x)$. So in the case of a partially degraded data instance the sum of the dot product and the bias parameter will be equal to or larger to zero and in the opposite case less or equal to zero. Now by definition there will exist a least one set of values for $\bar{w}$ such that the function in (5) satisfies that $y(x_n) > 0$ for $t_n = 1$ and $y(x_n) < 0$ for $t_n = -1$, which conveniently leads to $t_n y(x_n) > 0$ for all data instances.

As stated previously, the SVM chooses the decision boundary, which will ensure that the margin is maximized. The concept of distance from a point to a hyperplane can be exploited to state an maximization argument as $|y(x)/||w||$, where $w$ is the width of the decision surface. Additionally, as we are only interested in correctly classified points, which satisfies $t_n y(x_n) > 0$ for all $n$, we can state the distance of a point to the surface as

$$\frac{t_n y(x_n)}{||w||} = \frac{t_n(w^T \phi(x_n) + b)}{||w||} \tag{6}$$

The distance can be stated as an optimization argument that optimizes the parameters $b$ and $w$ in order to maximize the margin

$$\max_{w,b} \left\{ \frac{1}{||w||} \min_n [t_n(w^T \phi(x_n) + b)] \right\} \tag{7}$$

An explicit solution of (7) is quite complex to obtain, so the expression is rescaled such that the nearest data point has a distance of one. Let $w \rightarrow cw$ and $b \rightarrow cb$ so that

$$\min_n t_n(w^T \phi(x_n) + b) = 1 \tag{8}$$

Now the optimization problem is simply reduced to maximizing $||w||^{-1}$, which is equivalent to minimizing $||w||$ and the problem can therefore be stated as

$$\min_w \frac{1}{2}||w||^2 \tag{9}$$

and since the closest data point is one, the minimization has to honour the following constraint

$$t_n(w^T \phi(x_n) + b) \geq 1 \tag{10}$$

This is known as the primal form of SVM, which is formed on the basis of assuming that the data is perfectly separable and that all data points are classified correctly. In practice, however, the condition class distributions may overlap, as depicted in Fig. 10, and exact separation can then lead to poor generalization. The approach is therefore modified in such a way that data points are now allowed to be located within the margin boundary, but at the same time with added penalty, which increases as the distance to the boundary increases. For the mathematical convenience of the subsequent optimization problem, the penalty is chosen to be a linear function of the distance as $\zeta_n \geq 0$ and has contribution of $\zeta_n \geq 1$ in case of

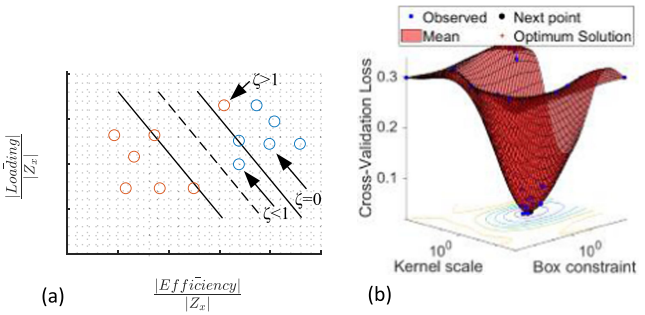


**FIGURE 13.** (a): Illustration of the concept of including slack variables for soft margin classification. (b): Cross-validation loss evaluation for different set of box constraint and kernel scale.

misclassifications as shown in Fig. 13(a) [29]. This concept is commonly referred to as soft margin as it relaxes the hard margin constraint, which can be stated as

$$t_n(w^T \phi(x_n) + b) \geq 1 - \zeta_n \tag{11}$$

The optimization goal has now changed to maximize the margin while penalizing the data points that are located at the wrong side of the boundary. The minimization problem stated in expression (9) is adapted to include misclassification slack

$$\min_w C \sum_{n=1}^{N} \zeta_n + \frac{1}{2}||w||^2 \tag{12}$$

where $C$ is the box constraint that controls the degree of trade-off between the induced penalty and the margin. In case of $C$=0, the classifier is not penalized by slack and hence the optimization can afford to use it anywhere and even large misclassification would be acceptable. This would result in a linear decision boundary and would therefore lead to underfitting. In contrast, an infinitely high C value will result in that even a small slack is highly penalized so the classifier cannot afford to misclassify a data point, which leads to complex decision boundaries and hence overfitting. This is a case of a convex quadratic optimization problem as we are dealing with a quadratic objective function subjected to linear constraints. In order to solve a constrained optimization problem the method of Lagrance multipliers are applied. The corresponding Lagrangian function is given by

$$L = (w, b, \zeta, \alpha, \lambda) = \frac{1}{2}||w||^2 + C \sum_{n=1}^{N} \zeta_n - \sum_{n-1}^{N} \alpha_n [t_n y(x_n) - 1 + \zeta_n] - \sum_{n=1}^{N} \lambda_n \zeta_n \tag{13}$$

where $\alpha_n$ and $\lambda_n$ are the Lagrance multipliers. It is now desired to obtain the SVM in dual form, which eliminates the primal variables and thereby reduces the optimization problem to only being dependent on pairs of data points. In order to eliminate the primal variables, expression (13) is differentiated with respect to $w, b$ and $\zeta_n$ and set equal to zero. The obtained expressions are then used to eliminate those variables from

the Lagrangian and finally, the optimization problem in dual formulation is obtained [29]

$$\max_{\alpha_i} \left( \sum_{n=1}^{N} \alpha_n - \frac{1}{2} \sum_{n=1}^{N} \sum_{m=1}^{N} \alpha_n \alpha_m t_n t_m k(x_n, x_m) \right) \tag{14}$$

Where $k(x_n, x_m)$ denotes the kernel function which systematically determine SVMs in higher dimensions and thereby enables good separation properties of the classifier when dealing with linearly inseparable data. Due to the properties of kernelization it allows us to operate in the original two-dimensional space without computing the coordinates of the data in a higher dimensional space so the inner product only depends on the base features as described in (15).

$$k(x_n, x_m) = \phi(x_n) \cdot \phi(x_m) \tag{15}$$

where $\phi$ denotes the feature space transformation. The kernel used for this problem is known as the radial basis function, which can be expressed as

$$k(x_n, x_m) = exp\left(-\gamma ||x_n - x_m||^2\right) \tag{16}$$

where $\gamma$ is the scaling parameter used to scale the data as the kernel is evaluted [30]. Finally, we have an optimization problem which can be solved numerically with relatively ease. The problem consists of maximizing expression (14) with respect to $\alpha_n$ while subjected to

$$\sum_{n=1}^{N} \alpha_n t_n = 0 \tag{17}$$

$$0 \leq \alpha_n \leq C \tag{18}$$

The feature set is divided into training and test datasets while initially the full dataset is randomly permutated with the purpose of ensuring that the operating conditions from all seasons are represented in both the training and test datasets. Furthermore, a five-fold partition is made from the training data, which is used for cross-validation when training the model. This guarantees that the model achieves maximum utilization of the degradation data contained in the dataset. During training, the optimal values for the kernel scale $\gamma$ and the box constraint $C$ is obtained based on the ones that will minimize the cross-validation loss. The evaluation is depicted in Fig. 13(b) and resulted in $C = 11.761$ and $\gamma = 1.8711$. The model accuracy is subsequently evaluated by comparing the model outputs with known condition labels of the separate test dataset

$$Accuracy = \frac{\sum(\text{Model predictions}(x_{test}) == y_{test})}{N_{test}} \cdot 100 \tag{19}$$

where $x_{test}$ is the test feature set, $y_{test}$ is the known labels of the test feature set and $N_{test}$ is the size of the test feature set. In Fig. 14, where the solid dots represents the training data, encircled dots are the data used for support vectors and the crosses denotes the test data. It can be obeserved in the Fig. 14 that the hyperplane separates the health classes of the

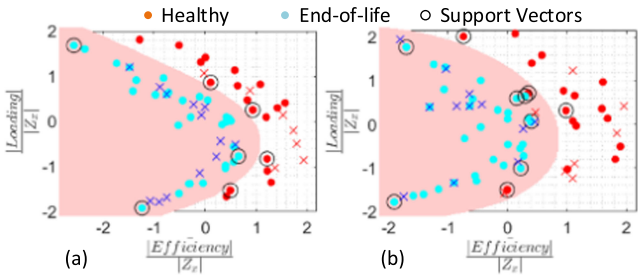


**FIGURE 14.** Visualization of the hyperplane separating the white and red areas in the feature space containing the standarised values of mean efficiency and mean loading. (a): Idealised results with 100 percent accuracy. (b): Case including measurement inaccuracies resulting in overlapping and 90 percent accuracy.

test observations one hundred percent correctly. It is quite obvious that the decision boundary resembles a tilted, normalized efficiency/loading curve, implying that the end-of-life detection perfectly overcomes the issue of the health precursors dependency on the applied operating conditions. The red area denotes the end-of-life of the converter at all conditions and the white area denotes the Safe Operational Area. The results in Fig. 14(a) are obtained during idealized conditions with an infinite amount of information available by simulating the system shown in Fig. 1. In order to obtain a more realistic impression of how the detection model performs in practical circumstances, measurement inaccuracies are taken into account. The simulation output of nearly 2 MHz resolution is downsampled to 20 kHz, which is a typical sampling rate of sensors used for prognostic purposes. With unlimited information the efficiency response is periodically averaged with respect to the fundamental frequency, which provides an efficiency signal value of constant amplitude. The loss of information caused by resampling to 20 kHz removes the possibility of obtaining perfect averaging and thereby introduces a measurement error of 0.03 percent. Additionally, 0.1 percent error is introduced by inherent sensor inaccuracies when using class 0.1 sensors and finally, Gaussian white noise is added to the efficiency response with a signal-to-noise ratio of 80. The errors are randomly added or subtracted the idealized data and the results can be observed in Fig. 14(b). As it can be observed in the Fig. 14(b), health classes overlap are starting to occur, which leads to some degree of misclassifications. But due to the use of soft margins, the individual cases of misclassification do not lead to hyperplanes with poor outcomes, due to the box constraint being regulated to gain maximum performance. This exact case led to two test observation misclassifications, which are the data instances labeled by red crosses, that are located within the end-of-life area. This amounts to an accuracy of 90 percent, which is still satisfying, when considering that there is no existing alternatives at this point.

## VI. CONCLUSION

Due to the high cost of failure related downtime of power converters operating in a wide variety of applications, it is essential to gain the ability of stating the lifetime with high

precision. There is a substantial amount of uncertainty linked to the existing PoF methodology, which can lead to inaccurate predictions. A promising alternative is PHM based methods where electro-thermal parameters are used as health indicators. Nevertheless, all existing methods are restricted to individual types of components, which is a severe limitation as degradation is likely to occur on multiple components concurrently. This paper proposes a method, which exploits the efficiency as an application-level health precursor, which enables the health monitoring of unified power converters. In addition, the issue of the effiency being dependent on the specific operating condition is dealt with by using a SVM based classifier for end-of-life detection. The SVM classifier is able to construct non-linear decision boundaries to overcome this dependency, while at the same time being computational efficient, by avoiding actual transformations into a higher dimensional space. To avoid concluding the results solely based on idealized conditions, the effect of measurement inaccuracies are taken into account, which led to some degree of overlapping. The effect of the individual misclassifications did not result in hyperplanes with poor outcomes, due to the use of soft margins and an optimal amount of introduced penalized slack. Finally, the method can be extended to include continuously updating remaining useful life estimations using the efficiency based features and also a method which takes the rate-of-change of efficiency into consideration as this will deal with the assumption of homogeneous degradation of all components. The remaining useful life estimations can provide advanced warning of failures, minimize unscheduled maintenance, extend maintenance cycles and maintain effectiveness through timely repairs. This will lead to a reduction in life-cycle cost by decreasing downtime and inspection costs.

## REFERENCES


[1] Z. Tang, Y. Yang, and F. Blaabjerg, "Power electronics: The enabling technology for renewable energy integration," *CSEE J. Power Energy Syst.*, vol. 8, no. 1, pp. 39–52, Jan. 2022.

[2] J. Falck, C. Felgemacher, A. Rojko, M. Liserre, and P. Zacharias, "Reliability of power electronic systems: An industry perspective," *IEEE Ind. Electron. Mag.*, vol. 12, no. 2, pp. 24–35, Jun. 2018.

[3] H. Wang et al., "Transitioning to physics-of-failure as a reliability driver in power electronics," *IEEE J. Emerg. Sel. Topics Power Electron.*, vol. 2, no. 1, pp. 97–114, Mar. 2014.

[4] A. Hanif, Y. Yu, D. DeVoto, and F. Khan, "A comprehensive review toward the state-of-the-art in failure and lifetime predictions of power electronic devices," *IEEE Trans. Power Electron.*, vol. 34, no. 5, pp. 4729–4746, May 2019.

[5] H. Wang and F. Blaabjerg, "Power electronics reliability: State of the art and outlook," *IEEE J. Emerg. Sel. Topics Power Electron.*, vol. 9, no. 6, pp. 6476–6493, Dec. 2021.

[6] R. Bayerer, T. Herrmann, T. Licht, J. Lutz, and M. Feller, "Model for power cycling lifetime of IGBT modules - various factors influencing lifetime," in *Proc. 5th Int. Conf. Integr. Power Electron. Syst.*, 2008, pp. 1–6.

[7] J. Gu and M. Pecht, "Uncertainty assessment of prognostics of electronics subject to random vibration," in *Proc. AAAI Fall Symp.: Artif. Intell. Prognostics*, 2007, pp. 1330–1334.

[8] A. Sangwongwanich, Y. Yang, D. Sera, and F. Blaabjerg, "Mission profile-oriented control for reliability and lifetime of photovoltaic inverters," *IEEE Trans. Ind. Appl.*, vol. 56, no. 1, pp. 601–610, Jan./Feb. 2020.

[9] D. Zhou, G. Zhang, and F. Blaabjerg, "Optimal selection of power converter in DFIG wind turbine with enhanced system-level reliability," *IEEE Trans. Ind. Appl.*, vol. 54, no. 4, pp. 3637–3644, Jul./Aug. 2018.

[10] Y. Avenas, L. Dupont, N. Baker, H. Zara, and F. Barruel, "Condition monitoring: A decade of proposed techniques," *IEEE Ind. Electron. Mag.*, vol. 9, no. 4, pp. 22–36, Dec. 2015.

[11] X. Perpiñà et al., "Reliability and lifetime prediction for IGBT modules in railway traction chains," in *Reliability and Safety in Railway*, X. Perpinya, Ed. InTech, 2019. [Online]. Available: http://www.intechopen.com/books/reliabilityandsafetyinrailway

[12] W. Wu, M. Held, P. Jacob, P. Scacco, and A. Birolini, "Investigation on the long term reliability of power IGBT modules," in *Proc. Int. Symp. Power Semicond. Devices IC's*, 1995, pp. 443–448.

[13] M. Bouarroudj et al., "Degradation behavior of 600 V-200 A IGBT modules under power cycling and high temperature environment conditions," *Microelectronics Rel.*, vol. 47, pp. 1719–1724, 2007.

[14] L. Dupont, S. Lefebvre, M. Berkani, Z. Khatir, and J. C. Faugières, "Failure modes on low voltage power MOSFETs under high temperature application," *Microelectronics Rel.*, vol. 47, pp. 1767–1772, Jul. 2007.

[15] A. Hamidi, N. Beck, K. Thomas, and E. Herr, "Reliability and lifetime evaluation of different wire bonding technologies for high power IGBT modules," *Microelectronics Rel.*, vol. 39, no. 6, pp. 1153–1158, 1999.

[16] P. Jacob, M. Held, P. Scacco, and W. Wu, "Reliability testing and analysis of IGBT power semiconductor modules," *IEE Colloq. IGBT Propulsion Drives*, pp. 4/1–4/5, 1995.

[17] P. Cova and F. Fantini, "On the effect of power cycling stress on IGBT modules," *Microelectronics Rel.*, vol. 38, no. 6, pp. 1347–1352, 1998.

[18] D. C. Katsis and J. D. Van Wyk, "Experimental measurement and simulation of thermal performance due to aging in power semiconductor devices," in *Proc. IEEE 37th IAS Annu. Meeting Conf. Rec. Ind. Appl.*, 2002, vol. 3, pp. 1746–1751.

[19] H. Oh, B. Han, P. McCluskey, C. Han, and B. D. Youn, "Physics-of-failure, condition monitoring, and prognostics of insulated gate bipolar transistor modules: A review," *IEEE Trans. Power Electron.*, vol. 30, no. 5, pp. 2413–2426, May 2015.

[20] Z. Zhao, P. Davari, W. Lu, H. Wang, and F. Blaabjerg, "An overview of condition monitoring techniques for capacitors in DC-Link applications," *IEEE Trans. Power Electron.*, vol. 36, no. 4, pp. 3692–3716, Apr. 2021.

[21] T. Krone, L. Dang Hung, M. Jung, and A. Mertens, "Advanced condition monitoring system based on on-line semiconductor loss measurements," in *Proc. IEEE Energy Convers. Congr. Expo.*, 2016, pp. 1–8.

[22] T. Harder et al., "ECPE—Guideline AQG 324, qualification of power modules for use in power electronic converter units in motor vehicles," ECPE Online Tutorial, 2019.

[23] D. Sera, R. Teodorescu, and P. Rodriguez, "PV panel model based on datasheet values," in *Proc. IEEE Int. Symp. Ind. Electron.*, 2007, pp. 2392–2396.

[24] A. Sangwongwanich, Y. Yang, D. Sera, and F. Blaabjerg, "Lifetime evaluation of grid-connected PV inverters considering panel degradation rates and installation sites," *IEEE Trans. Power Electron.*, vol. 33, no. 2, pp. 1225–1236, Feb. 2018.

[25] H. Wang, P. Davari, H. Wang, D. Kumar, F. Zare, and F. Blaabjerg, "Lifetime estimation of DC-Link capacitors in adjustable speed drives under grid voltage unbalances," *IEEE Trans. Power Electron.*, vol. 34, no. 5, pp. 4064–4078, May 2019.

[26] Y. Fu, J. Zhu, S. Wang, and Z. Xi, "Reduced complexity SNR estimation via Kolmogorov-Smirnov test," *IEEE Commun. Lett.*, vol. 19, no. 9, pp. 1568–1571, Sep. 2015.

[27] S. Tong and D. Koller, "Restricted bayes optimal classifiers," in *Proc. 17th Nat. Conf. Artif. Intell. 12th Conf. Innov. Appl. Artif. Intell.*, 2000, 658–664.

[28] B. Schölkopf, A. J. Smola, R. C. Williamson, and P. L. Bartlett, "New support vector algorithms," *Neural Computation*, vol. 12, no. 5, pp. 1207–1245, May 2000.

[29] C. Cortes and V. Vapnik, "Support vector networks," *Mach. Learn.* vol. 20, pp. 273–297, 1995.

[30] B. Boser, I. Guyon, and V. Vapnik, "A training algorithm for optimal margin classifiers," in *Proc. 5th Annu. Workshop Comput. Learn. Theory*, 1992, pp. 144–152.

**MARTIN VANG KJÆR** (Student Member, IEEE) received the B.Sc. and M.Sc. degrees in energy technology with specializing in electrical energy engineering and power electronics and drives from Aalborg University, Aalborg, Denmark, in 2017 and 2020, respectively, where he is currently working toward the Ph.D. degree in applied power electronics with the Department of Energy. His research interests include intellingent power processing, reliable opertation of distributed generation systems, and prognostics and health management of power converters.

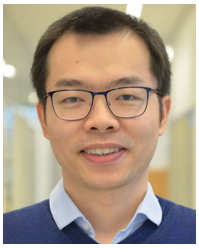

**HUAI WANG** (Senior Member, IEEE) received the B.E. degree in electrical engineering from the Huazhong University of Science and Technology, Wuhan, China, in 2007, and the Ph.D. degree in power electronics from the City University of Hong Kong, Hong Kong, in 2012. He is currently a Professor with AAU Energy, Aalborg University, Aalborg, Denmark, where he leads the Group of Reliability of Power Electronic Converters (ReliaPEC) and the mission on Digital Transformation and AI. He was a Visiting Scientist with ETH Zurich, Switzerland, from August to September 2014, and with the Massachusetts Institute of Technology, Cambridge, MA, USA, from September to November 2013. He was with the ABB Corporate Research Center, Switzerland in 2009. His research interests include the fundamental challenges in modeling and validation of power electronic component failure mechanisms and application issues in system-level predictability, condition monitoring, circuit architecture, and robustness design. Dr. Wang was the recipient of the Richard M. Bass Outstanding Young Power Electronics Engineer Award from the IEEE Power Electronics Society in 2016, and the Green Talents Award from the German Federal Ministry of Education and Research in 2014. He is the Chair of IEEE PELS/IAS/IES Chapter in Denmark. He is also an Associate Editor for *IET Electronics Letters*, IEEE JOURNAL OF EMERGING AND SELECTED TOPICS IN POWER ELECTRONICS, and IEEE TRANSACTIONS ON POWER ELECTRONICS. posium Paper Award in 2011.

**FREDE BLAABJERG** (Fellow, IEEE) received the Ph.D. degree in electrical engineering from Aalborg University, Aalborg, Denmark, in 1995. From 1987 to 1988, he was with ABB-Scandia, Randers, Denmark. He became an Assistant Professor in 1992, an Associate Professor in 1996, and a Full Professor of power electronics and drives in 1998 with AAU Energy. In 2017, he became a Villum Investigator. He is honoris causa with University Politehnica Timisoara, Timisoara, Romania, in 2017, and Tallinn Technical University, Tallinn, Estonia, in 2018. He has authored or coauthored more than 600 journal papers in the fields of power electronics and its applications. His research interests include power electronics and its applications, such as in wind turbines, PV systems, reliability, harmonics, and adjustable speed drives. He is the coauthor of four monographs and the Editor of ten books in power electronics and its applications. He was the recipient of 33 IEEE Prize Paper Awards, IEEE PELS Distinguished Service Award in 2009, EPE-PEMC Council Award in 2010, IEEE William E. Newell Power Electronics Award 2014, Villum Kann Rasmussen Research Award 2014, Global Energy Prize in 2019, and 2020 IEEE Edison Medal. He was the Editor-in-Chief of the IEEE TRANSACTIONS ON POWER ELECTRONICS from 2006 to 2012. He was a Distinguished Lecturer of the IEEE Power Electronics Society from 2005 to 2007 and IEEE Industry Applications Society from 2010 to 2011 and 2017 to 2018. During 2019–2020, he was a President of IEEE Power Electronics Society. He is the Vice-President of the Danish Academy of Technical Sciences. He is nominated in 2014-2020 by Thomson Reuters to be between the most 250 cited researchers in Engineering in the world.